Journal of Applied Remote Sensing

RemoteSensing.SPIEDigitalLibrary.org

Geostationary Operational Environmental Satellite Imager infrared channel-to-channel co-registration characterization algorithm and its implementation in the ground system

Zhenping Li
Michael Grotenhuis
Xiangqian Wu
Timothy J. Schmit
Chris Schmidt
Anthony J. Schreiner
James P. Nelson, III
Fangfang Yu
Hyre Bysal

SPIE.

Geostationary Operational Environmental Satellite Imager infrared channel-to-channel co-registration characterization algorithm and its implementation in the ground system

Zhenping Li,[a,*] Michael Grotenhuis,[b] Xiangqian Wu,[b] Timothy J. Schmit,[c] Chris Schmidt,[d] Anthony J. Schreiner,[d] James P. Nelson III,[d] Fangfang Yu,[b] and Hyre Bysal[e]

[a]ASRC Federal, 7515 Mission Drive, Seabrook, Maryland 20706, United States
[b]ERT Inc. @ NOAA/NESDIS/STAR, 5830 University Research Court, College Park, Maryland 20740, United States
[c]NOAA/NESDIS Office of Satellite Applications and Research, Advanced Satellite Products Branch (ASPB), Madison, Wisconsin 53706, United States
[d]University of Wisconsin-Madison, Cooperative Institute for Meteorological Satellite Studies, Space Science and Engineering Center, Madison, Wisconsin 53706, United States
[e]NOAA/NESDIS/OSPO, NSOF 1315 East West Highway, Silver Spring, Maryland 20910-3282, United States

Abstract. Channel-to-channel co-registration is an important performance metric for the Geostationary Operational Environmental Satellite (GOES) Imager, and large co-registration errors can have a significant impact on the reliability of derived products that rely on combinations of multiple infrared (IR) channels. Affected products include the cloud mask, fog and fire detection. This is especially the case for GOES-13, in which the co-registration error between channels 2 (3.9 μm) and 4 (10.7 μm) can be as large as 1 pixel (or ~4 km) in the east-west direction. The GOES Imager IR channel-to-channel co-registration characterization (GII4C) algorithm is presented, which allows a systematic calculation of the co-registration error between GOES IR channel image pairs. The procedure for determining the co-registration error as a function of time is presented. The algorithm characterizes the co-registration error between corresponding images from two channels by spatially transforming one image using the fast Fourier transformation resampling algorithm and determining the distance of the transformation that yields the maximum correlation in brightness temperature. The GII4C algorithm is an area-based approach which does not depend on a fixed set of control points that may be impacted by the presence of clouds. In fact, clouds are a feature that enhances the correlations. The results presented show very large correlations over the majority of Earth-viewing pixels, with stable algorithm results. Verification of the algorithm output is discussed, and a global spatial-spectral gradient asymmetry parameter is defined. The results show that the spatial-spectral gradient asymmetry is strongly correlated to the co-registration error and can be an effective global metric for the quality of the channel-to-channel co-registration characterization algorithm. Implementation of the algorithm in the GOES ground system is presented. This includes an offline component to determine the time dependence of the co-registration errors and a real-time component to correct the co-registration errors based on the inputs from the offline component. [DOI: 10.1117/1.JRS.8.083530]

Keywords: co-registration; image resampling; Geostationary Operational Environmental Satellite.

Paper 14451 received Jul. 30, 2014; revised manuscript received Sep. 11, 2014; accepted for publication Oct. 13, 2014; published online Nov. 6, 2014.

*Address all correspondence to: Zhenping Li, E-mail: Zhenping.Li@noaa.gov

1 Introduction

Co-registration, or the assurance that measurements from multiple channels are from the same geolocation, is an important performance metric for the Imager instrument on the Geostationary Operational Environmental Satellite (GOES). A number of satellite products rely on the difference between spectral measurements to infer the underlying geophysical parameter. For example, water vapor absorption is weaker in the 3.9 μm band (GOES Imager channel 2) than in the 10.7 μm band (channel 4) such that Tb(2), the brightness temperature for channel 2, is typically warmer than Tb(4) during nighttime hours. A brightness temperature (K) is uniquely related to the radiance via the Planck function. On the other hand, the emissivity of water droplets is lower in the 3.9 μm band than in the 10.7 μm band, which can lead to a cooler Tb(2) than Tb(4) in the presence of fog or low clouds. These properties have been used for fog water cloud detection.[1] However, if the channels have large co-registration errors, then measurements in the two channels can differ because they are from different locations. For example, the 3.9 μm band could be over water, while the 10.7 μm band could be over land (over vice versa). This can lead to misinterpretation of the measurements, such as false positives, in the fog detection product (Fig. 1).

A study by Cooperative Institute for Meteorological Satellite Studies personnel, as well as Grotenhuis et al.,[2] found that the co-registration error between channels 2 (3.9 μm) and 4 (10.7 μm) could be as large as 1 pixel in the east/west direction (or ~4 km), which is considerably larger than the instrument specification. Characterization of GOES channel to channel co-registration errors was seen as an important problem to solve.

Unlike most of the image registration problems discussed in the literature, the GOES Imager infrared (IR) channel-to-channel co-registration problem has its own unique characteristics. The images in different IR channels represent different radiometric attributes of the Earth-atmosphere system, and they are not related by simple affine (linear) transformations. Therefore, there is no controlled experiment to determine the accuracy of the algorithm output. The co-registration errors are generally at the subpixel level, which requires that one of the images be resampled in order to evaluate the co-registration error. An accurate resampling algorithm is crucial for a reliable co-registration error characterization algorithm. Furthermore, the co-registration error for GOES images is time dependent, and the determination of the co-registration error as a function of time is critical for the implementation of the algorithm in the GOES ground system. The focus of this paper is to present the GOES Imager IR channel-to-channel co-registration

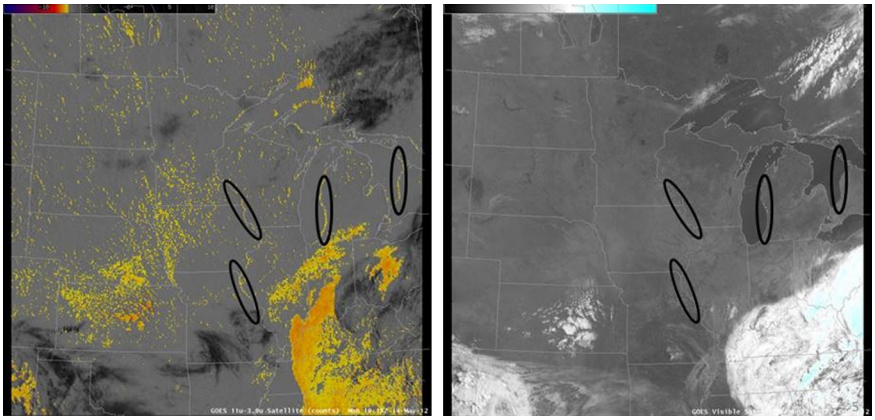

Fig. 1 Map of fog and low clouds based on the brightness temperature difference between Geostationary Operational Environmental Satellite (GOES)-13 Imager band 2 (3.9 μm) and band 4 (10.7 μm) for May 14, 2012, at 10:15 UTC. The colored regions denote where Tb(2) – Tb(4) is sufficiently negative, which is often indicative of the presence of low cloud and/or fog. Note the narrow lines of fog in the four marked regions along the Mississippi River and the shorelines of Lake Michigan and Lake Huron, where surface stations did not report fog or low clouds at the time. These were caused by the misalignment or co-registration error of the Imager measurement, when band 2 instantaneous field of view is a few kilometers east to that of band 4. As such, band 2 views the relatively cold land when band 4 views the relatively warm water in these early morning hours, which led to the negative Tb(2) – Tb(4) and false fog identification.

characterization (GII4C) algorithm, its validation and verification, and its implementation in the GOES ground system.

Although there are numerous algorithms that discuss image registration in medical imaging and remote sensing literature, few attempts have been made to characterize the channel-to-channel co-registration error. An initial attempt for the GOES Imager was made by Wu et al.,[3] who used the asymmetry in spatial versus spectral brightness temperature gradient histograms to identify the existence of co-registration errors. Le Moigne et al.[4] investigated the GOES channel-to-channel co-registration problem by using wavelets to extract certain features, or control points (CP), such as landmarks on images from different channels, which is an approach that has been widely used in image registration. A major problem for this approach is that it is not always possible to extract features on GOES images due to the presence of clouds, which makes it less reliable for a systematic evaluation of co-registration errors. A recent study by Grotenhuis et al.[2] uses an area-based approach that involves calculating the cross-correlation of Earth-viewing pixels in different IR channels. In this approach, one of the two images from different IR channels is resampled using linear interpolation, and the correlation in brightness temperature between the resampled image and the image from the other channel is computed. The shift that yields the maximum correlation is the negative of the co-registration error.

The GII4C algorithm uses the same approach as Grotenhuis et al.[2]— an area based approach to calculate correlations between images in different channels for Earth-viewing pixels. The key difference between this algorithm and the one in Ref. 2 is that fast Fourier transformation resampling (FFTR)[5] is used for the image resampling. The FFTR algorithm has been shown to be accurate, reversible, and efficient enough for spacecraft image resampling. It does not have the discontinuity problem for the correlation function seen with the images being resampled using linear interpolation.[2] Using the fast Fourier transform (FFT) to resample an image for the purpose of co-registration has been investigated in the literature.[6] A common issue with the FFT in subpixel image registration is the aliasing effects that cause the resampled image to be distorted. To avoid this problem, the Fourier spectrum for both images has to be truncated before the estimate of the co-registration error is made. However, the study in Ref. 5 shows that the Fourier spectra for GOES images are very well behaved, especially for channel 4 images, in which the Fourier spectrum is dominated by the low-frequency components, while the high-frequency components that cause the aliasing effects are very small. The aliasing effects do appear occasionally in the channel 2 images, in which the presence of fires, solar reflections, volcanoes, and other heat sources, such as cities, causes individual pixels to appear as high-temperature discontinuities in the spatial domain. An attempt to locate pixels containing actively burning fires and treat them separately to avoid the aliasing effects was made in Ref. 5. For the GII4C algorithm being presented, the images in channel 4 are resampled so that truncation of the Fourier spectrum is not necessary. The images in channel 2 are unchanged. This makes the algorithm simpler.

The validation and verification of the algorithm presents another challenge in characterizing the channel-to-channel co-registration errors since there is no controlled experiment to determine the accuracy of the algorithm. This has not been investigated in the literature. To verify the output of the GII4C algorithm, the channel 4 images have to be resampled based on the co-registration errors obtained from the GII4C algorithm itself. One can examine local features on the resampled image to determine if the co-registration error has been corrected. However, the study of local features alone is not sufficient to determine the overall image quality improvements, and global measures are needed to provide a quantitative description of such improvements. Because the correlations between images in different channels are driven by features with large temperature gradients, the spatial and spectral gradient approach proposed in Ref. 3 is a very useful representation for highlighting the co-registration error effects. The spectral gradient mean and standard deviation as a function of the temperature gradient provide quantitative indicators of co-registration errors. Our study shows that the co-registration error leads to an asymmetric behavior of the spectral gradient mean function that is in agreement with the conclusion in Ref. 3. A global spatial-spectral gradient asymmetry parameter is defined in terms of the spectral gradient mean function, which is strongly correlated to the co-registration errors and is a useful quantitative metric for the effectiveness of channel-to-channel co-registration characterization algorithms.

This article is organized as follows. Section 2 briefly discusses the FFTR algorithm. Section 3 provides detailed discussions of the GII4C algorithm. Section 4 shows how the algorithm works for a specific set of GOES images. Section 5 presents the mean and standard deviation of the spectral gradient as a function of the spatial gradient, and how these measures can be used as quantitative metrics for the overall improvement of data quality due to co-registration error corrections. The determination of the co-registration error as a function of time, which is crucial to the implementation of the GII4C algorithm in the GOES ground system, is discussed in Sec. 6. Finally, the summary is given in Sec. 7.

2 FFTR Algorithm

As was outlined by Li,[5] an image can be characterized by a two-dimensional array, with each element $P_{i,j}$ specifying a pixel value at a location $\{i, j\}$. Image resampling involves finding an array with elements $P_{i+\delta_i,j+\delta_j}$ at locations $\{i+\delta_i, j+\delta_j\}$ based on the input array $P_{i,j}$, where i and j are both integers and δ_i and δ_j are generally both fractional numbers. Generally, resampling in δ_i and δ_j directions can be performed separately. Therefore, we will focus our discussion on resampling in one dimension, which can then be easily extended to two dimensions.

For one-dimensional resampling, one can define a global continuous function $G(x)$ with the condition

$$G(i) = P_i \quad \text{for } 0 \le i \le N-1, \tag{1}$$

so that one can find the resampled line

$$P_i^{\delta} = G(i+\delta) \quad \text{for } 0 \le i \le N-1, \tag{2}$$

where P_i is a one-dimensional array with size N. To satisfy the condition in Eq. (1), one can use the discrete Fourier transformation

$$G_x = P_0 + \sum_{k=0}^{M-1} g(k) \sin\left(\frac{\pi k x}{M}\right), \tag{3}$$

with the reverse transformation

$$g(k) = \frac{2}{M} \sum_{x=0}^{M-1} [G(x) - P_0] \sin\left(\frac{\pi k x}{M}\right), \tag{4}$$

where P_0 is the first element of the input array P_i. Because the array P_i from an image is real, the real sine or cosine function is used in the Fourier expansion, which ensures real values for the resampled array.

In order to use the FFT algorithm, the dimension of an input array has to meet the size requirement $M = 2^m$ for the integer m. The global function $G(x)$ in Eq. (3) from the FFT is related to the input array as

$$G(i) = \begin{cases} P_i & \text{for } 0 \le i \le N \\ P_{2\,N-i-1} & \text{for } N \le i \le M/2 \\ G(M-x) & \text{for } M/2 \le i \le M \end{cases}, \tag{5}$$

where

$$M = 2^m \quad \text{and} \quad m = \text{INT}\left(\frac{\log N}{\log 2}\right) + 2. \tag{6}$$

Therefore, one can use Eq. (4) to obtain the amplitude $g(k)$. The resampled array P_i can be obtained by adding a phase shift δ to the Fourier expansion in Eq. (3).

$$P_i^{\delta} = P_0 + \sum_{k=0}^{M-1} g(k) \sin\left[\frac{\pi(i+\delta)k}{M}\right]. \tag{7}$$

For an integer δ, Eq. (7) becomes

$$P_i^{\delta} = P_{i+\delta}. \tag{8}$$

The elements at i of the resampled array are equal to the element at $i + \delta$ of the input array, which should be generally true for any resampling algorithm.

For a noninteger δ, Eq. (7) cannot be directly used in the FFT because the argument of the sine function no longer has the form of a standard discrete transform, and direct calculation of Eq. (7) has an efficiency of $O(N^2)$ for a one-dimensional array. In order to use the FFT, Eq. (7) is rewritten as

$$P_i^{\delta} = P_0 + \sum_{k=0}^{M-1} g_{\delta}^{S}(k) \sin\left(\frac{\pi k i}{M}\right) + \sum_{k=0}^{M-1} g_{\delta}^{c}(k) \cos\left(\frac{\pi k i}{M}\right), \tag{9}$$

with

$$g_{\delta}^{S}(k) = g(k) \cos\left(\frac{\pi k \delta}{M}\right). \tag{10}$$

and

$$g_{\delta}^{C}(k) = g(k) \sin\left(\frac{\pi k \delta}{M}\right). \tag{11}$$

This global function with a phase shift can be evaluated with two separate FFTs. The steps for FFTR are as follows:

1. Construct an array in FFT using Eq. (5).
2. Perform the FFT to obtain $g(k)$ using Eq. (4).
3. Construct arrays $g_{\delta}^{S}(k)$ and $g_{\delta}^{C}(k)$ using Eqs. (10) and (11).
4. Perform two FFT computations for $g_{\delta}^{S}(k)$ and $g_{\delta}^{C}(k)$.
5. Generate the resampled array P_i^{δ} using Eq. (9).

The c routines for the sine and cosine function FFTs come from Ref. 7.

Both resampled and original images belong to the same global continuous function with the same set of Fourier spectra. The resampled images from the FFTR algorithm maintain the image quality of the original images, which are supported by independent studies.[8] Furthermore, the FFTR algorithm is generally reversible. One could simply treat the resampled image with the shift δ as the original image to derive the global function and regenerate the original image by performing the image resampling with the shift δ. A special test case is the integer shift, as the resampled image data at the position (i, j) correspond directly to the original image data at the position $(i + \delta, j)$ for the integer shift δ along the x-direction.

3 GII4C Algorithm

The GOES Imager instrument senses images of Earth with both visible and IR channels. The GOES Imager has one visible and four IR channels.[9] The four IR channels for the current generation of GOES have wavelengths 3.9, 6.5, 10.7, and 13.3 μm, which are identified as channels 2, 3, 4, and 6, respectively. Assuming that channel 4 is used as the reference channel, a pixel with coordinates $\{i, j\}$ on an image corresponds to the geolocation $\{\theta, \varphi\}$ on Earth, where θ and φ represent latitude and longitude, respectively. The same geolocation $\{\theta, \varphi\}$ would correspond to $\{i + \delta_i^C, j + \delta_j^C\}$ for channels $C = 2$, 3, and 6, where δ_i^C and δ_j^C are the co-registration errors in the east/west and north/south directions, respectively.

The GII4C algorithm uses the same approach as that described by Grotenhuis et al.[2] It is an area-based approach based on characteristics of the GOES images that do not depend on a specific set of CP. The interpolation that best correlates brightness temperature between the two channels is used to estimate the co-registration error. Using correlation to evaluate the co-registration errors has been shown to be one of the best approaches.[10] This is especially true for GOES images in IR channels, as they are different images not related by the affine transformation, but nonetheless display similar features. The algorithm calculates the correlation line by line or column by column. For a given line j in the images of two IR channels, this correlation function can be written as

$$R_j(\delta) = \frac{\sum_{i=0}^{N-1} [T_C(i) - \overline{T_C}][T_4(i+\delta) - \overline{T_4}]}{\sqrt{\sum_{i=0}^{N-1} [T_C(i) - \overline{T_C}]^2 \sum_{i=0}^{N-1} [T_4(i+\delta) - \overline{T_4}]^2}}, \tag{12}$$

where $T_C(x)$ is the brightness temperature at pixel x from channel C and $\overline{T_C}$ is the mean value of the brightness temperature for line j in channel C. The brightness temperature $T_C(x)$ for channel C can be derived from the pixel value from the IR image.[11] The temperature $T_4(i+\delta)$ is obtained by the FFTR based on the input of $T_4(i)$. The correlation coefficient $R_j(\delta)$ is a function of the co-registration error δ. For the image registration problem, the correlation coefficient $R_j(\delta)$ has a range between 0 and 1 in brightness temperature correlations via Eq. (12), where 0 corresponds to no correlation and 1 corresponds to a perfect linear correlation.

The value for the co-registration error δ_j^C at line j corresponds to the maximum correlation $R_j(\delta)$. Equation (12) shows that the correlation function $R_j(\delta)$ depends on the variation of the temperature from the mean value. A large correlation value requires that a line in an image have a large brightness temperature variation, in which the difference between the maximum and minimum brightness temperature in a line is sufficiently large. This is not always true in a satellite image, and it depends on the content of the image. For example, if a line in a satellite image contains a large segment of space pixels, the brightness temperature would be nearly constant, and consequently, the correlation should be small. Thus, it is important to exclude the space segment data from the correlation calculation so that only Earth data are evaluated. The selection of Earth pixels from GOES images is based on navigation information typically provided along with the GOES image. A detailed formulism can be found in Ref. 12. The co-registration error for an image is the weighted average over the total number of lines in the image and should be used to obtain the channel-to-channel co-registration errors.

$$\delta^C = \frac{\sum_{j=0}^{M} \delta_j^C w_j}{\sum_{j=0}^{M} w_j}, \tag{13}$$

where

```
Convert the image of each IR channel into two dimensional temperature arrays
For each line in the temperature arrays
    Obtain the array with the elements on Earth
    Initialize the max correlation for channel 2, 3, 6 to 0.
    Initialize the shift for channel 2, 3, 6 with -100.0
    For each co-registration error from -2.0 to +2.0 increment by 0.1
        Perform the resampling using FFTR on channel 4 temperature array with the co-registration error.
        For each channel in 2, 3, 6
            Calculate the temperature correlation with channel 4 using Eq. 12.
            Compare the correlation with the max-correlation
                if the temperature correlation is larger
                    replace the max-correlation and the shift value for the line.
    If the max-correlation for the line in each channel is equal or larger than 0.8
            add it to the weighted mean for the image.
Obtain the co-registration error of the image using Eq. 13.
```

Fig. 2 The GOES Imager infrared channel-to-channel co-registration characterization algorithm.

$$w_j = \begin{cases} R_j(\delta_j^C) & \text{for } R_j(\delta_j^C) \geq 0.8 \\ 0 & \text{for } R_j(\delta_j^C) \geq 0.8 \end{cases}. \tag{14}$$

The threshold for a line to be included in the weighted mean of the image is 0.8. This ensures that the co-registration errors are determined from the lines with large correlations. The algorithm to measure the east/west channel-to-channel co-registration error is shown in Fig. 2.

4 Simulation Results

To demonstrate how the GII4C works with IR channel images from the GOES Imager, we will show the application of the algorithm to the IR channels 2 and 4 images shown in Figs. 3 and 4. This set of images covers the continental United States (CONUS) and was imaged at 12:15 UTC on ordinal day 136, 2012 (May 15, 2012). The image set dimensions are 3462 (east/west) by 1246 (north/south) pixels for both channels. Most GOES images acquired during normal operations have sizes that are either equal to or larger than the size of these images. The images contain both Earth and space pixels, with the space pixels located in the upper left and right corners of each image. Both images contain similar features; however, they represent different spectral regions of the Earth's atmosphere that are not defined by the affine transformations. Figure 5 shows the channels 2 and 4 brightness temperatures along a given image line in Figs. 3 and 4, and highlights the similarities and differences between these two channels. Both channels show similar features, in which the brightness temperature in both channels increases or decreases at the same time; however, the magnitude of the brightness temperature changes is not identical.

Figure 6 shows the Fourier spectrum of the channel 4 brightness temperatures in Fig. 4, where the x axis is defined as k/M, as shown in Eq. (9), and has a range from 0 to 1. The Fourier spectrum is dominated by the very low-frequency components, and it decreases very quickly to 0 as the frequency increases. The magnitude for the component $k = 1$ is ~ 3, while the magnitude for $k = M$ is $\sim 10^{-4}$. This makes frequency truncation in the resampling[4] unnecessary, as aliasing is not a concern for the channel 4 data. As a result, the GII4C algorithm becomes less complex since a Fourier transformation for the data in channel 2 is not needed.

Figure 7 shows the correlation as a function of δ for line 739. The correlation is essentially a statistical approach that requires a large data set to become mathematically stable. The size of the data set in this case is >1000 data points. The maximum value of the correlation is 0.89 at

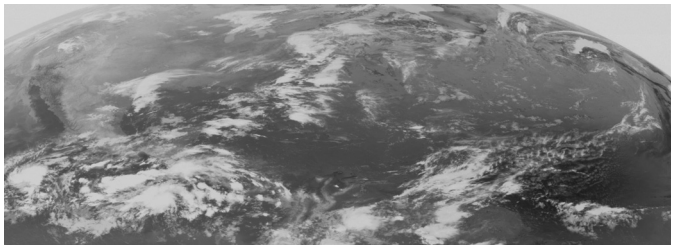

Fig. 3 Infrared (IR) channel 2 (3.9 μm) image from the GOES-13 Imager from 1215 UTC, May 15, 2012.

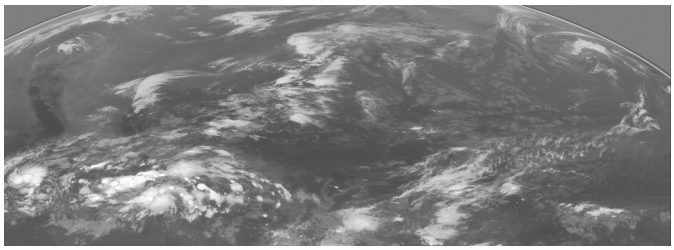

Fig. 4 IR channel 4 (10.7 μm) image from the GOES-13 Imager from 1215 UTC, May 15, 2012.

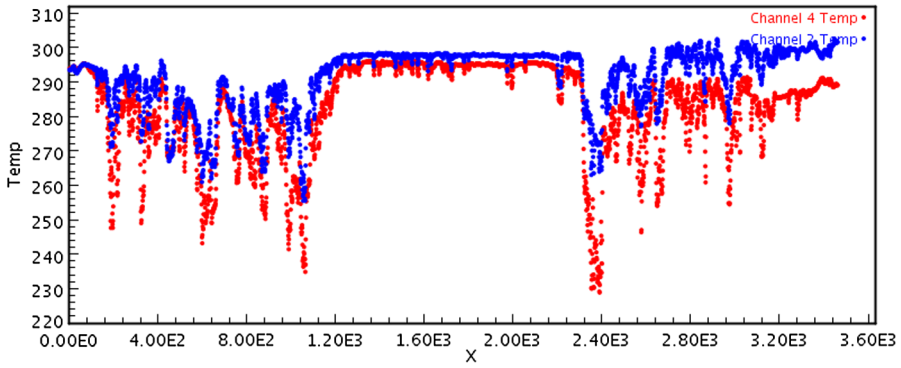

Fig. 5 Channel 2 (see Fig. 3) and 4 (see Fig. 4) brightness temperature for image line 739. The red data represent the brightness temperature in channel 4 and the blue data represent the brightness temperature in channel 2.

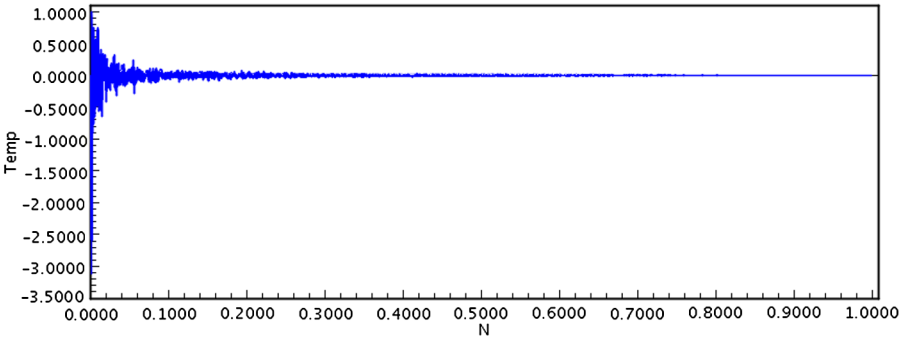

Fig. 6 The Fourier spectrum for the channel 4 brightness temperatures shown in Fig. 5.

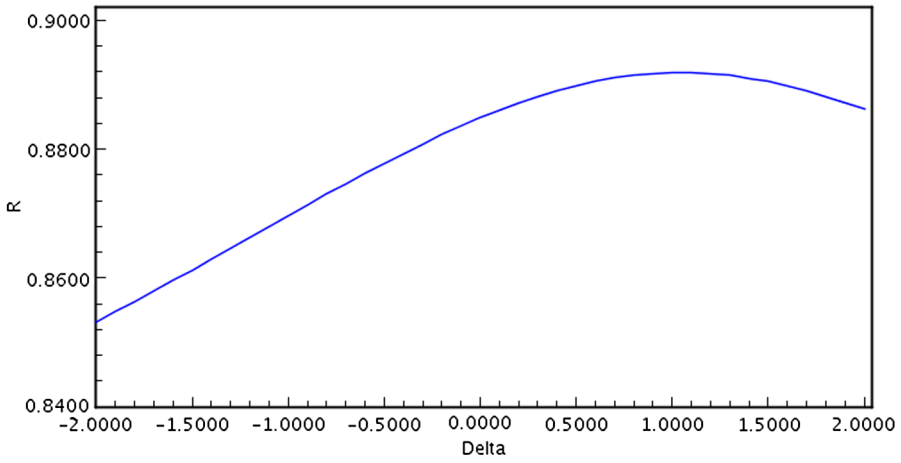

Fig. 7 Brightness temperature correlation as a function of δ (delta) at line 739. The brightness temperature data for channels 2 and 4 are shown in Fig. 5.

$\delta = 1.0$, which is considerably larger than the results presented in Ref. 4 using the feature-based approach with a much smaller data sample size.

Unlike the approach in Ref. 2 that uses linear interpolation for the image resampling, the GII4C algorithm uses the FFTR for the resampling. Figure 7 shows that the correlation function is continuous as a function of δ (delta); therefore, it does not require the scramble procedure described in Ref. 2.

Figure 8 shows the maximum correlation values as a function of line number for the channels 2 and 4 images shown in Figs. 3 and 4. The correlation is small for the top area of the images (far

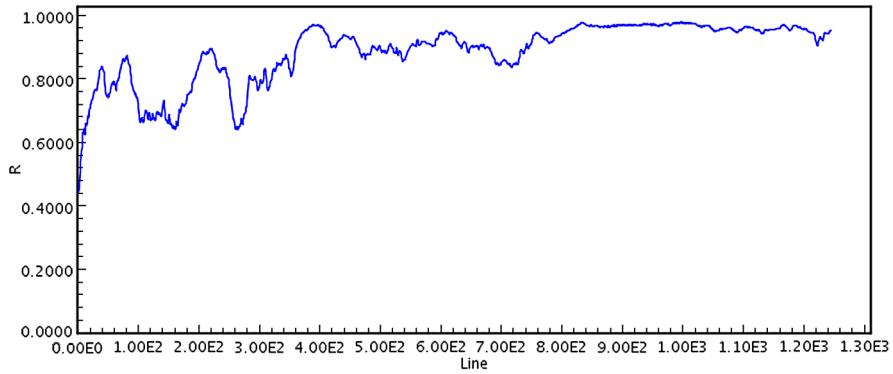

Fig. 8 Maximum correlation value as a function of line number for the channels 2 and 4 images shown in Figs. 2 and 3, respectively.

north latitudes), with a range from 0.4 to 0.6. The small correlation is due to the fact that the number of Earth pixels is relatively small because of the presence of space segments on either side of the Earth. The maximum correlation values become more stable when the image line number is larger than ∼400. The data show that as much as 80% of the lines in the images have a maximum correlation larger than the threshold (0.8) and are included in the weighted average in Eq. (13). The percentage of the number of lines above the 0.8 threshold is even larger for typical GOES-13 images, as the percentage of far northern and southern pixels is smaller than the CONUS image shown in Figs. 3 and 4. The largest value found for the maximum correlation is ∼0.95, which is a very strong correlation. The reasons for such a strong correlation in this approach are twofold. First, the size of the data set is much larger than that in the feature-based approach. More importantly, this approach includes many more image elements than the feature-based approach, which only selects a limited set of CP. In addition to coast lines and landmarks, clouds in the images also enhance the correlation. Figure 5 highlights the components included in the correlation calculation. There are many maximum and minimum peaks for a given line, and each peak contributes to the correlation between the two data sets. Figure 9 shows the corresponding co-registration error for each line. There is a relatively large fluctuation at the top of the images, where the maximum correlation value is small. As the maximum correlation value in Fig. 8 increases, the corresponding co-registration error becomes relatively stable with less fluctuation. Adopting a 0.8 threshold for the weighted average in Eq. (13) ensures a more stable outcome.

After using the data represented in Figs. 8 and 9 for the weighted average in Eq. (13), the final co-registration error for the image set is 1.17 pixels.

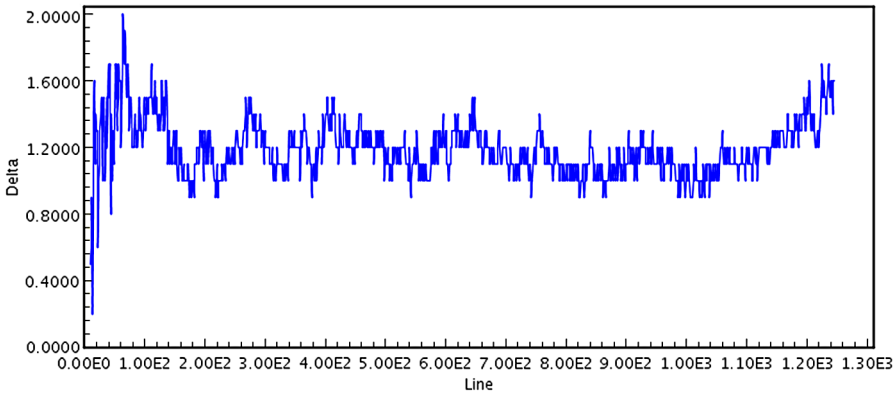

Fig. 9 Co-registration error corresponding to the maximum correlation as a function of line number.

5 Algorithm Verification and Validation

There are two main steps needed for algorithm updates. The first is the verification step, i.e., whether the update meets the specified requirement(s). The second step is the validation, where the deliverable is deemed suitable in the intended environment. Unlike algorithms in image registration, where the accuracy of an algorithm can be determined with a set of images with known image registration errors, there is no controlled experiment to determine the accuracy of the channel-to-channel co-registration characterization algorithm. To verify the GII4C algorithm, the channel 4 image has to be resampled with the shift determined by the GII4C algorithm, so that the features in different IR channels can be evaluated in terms of alignment. One possible approach is to examine local features, such as landmarks, to see if the co-registration error has been corrected. Unfortunately, this type of approach only provides qualitative answers. More desirable are quantitative measures that are sensitive to co-registration errors on a global scale. In this section, we present such quantitative measures related to brightness temperature differences between different channels that can be used as metrics for channel-to-channel co-registration characterization algorithms.

Since the channel 2 to 4 co-registration errors are also very sensitive to the brightness temperature difference (also called the spectral gradient), one can calculate the spectral gradient mean (m) and standard deviation (σ) values between channels, respectively, as

$$m = \frac{1}{N}\sum_i [T_2(i) - T_4(i)], \tag{15}$$

$$\sigma = \sqrt{\frac{1}{N}\sum_i [T_2(i) - T_4(i) - m]^2}, \tag{16}$$

where the summations in Eqs. (15) and (16) concern Earth-viewing pixels only. The σ values should be smaller for the more correlated channels 2 and 4 images, compared to less correlated images. The values m and σ for the original and resampled channel 4 image sets are shown in Table 1. The channel 4 images are resampled with the FFTR algorithm. The results show that the spectral gradient mean value remains mostly unchanged between the original and resampled imagery, whereas modestly larger changes occur in the σ values between the original and resampled imagery. The changes to the σ values become more significant as the magnitude of the co-registration error increases.

Table 1 shows that the changes to the σ value for the image as a whole are relatively small. This is due to the fact that the differences between the resampled and original images are only significant where the features (such as landmarks or coast lines) are located. Mathematically, the difference between the original and resampled images at a given location is proportional to the temperature gradient. This is defined as

$$g_C(i) = T_C(i+1) - T_C(i), \tag{17}$$

which is the difference between neighboring pixels along a given line for a channel C image. Equation (17) defines the temperature gradient along the east/west direction. Similarly, one could also define the gradient along the north/south direction for a given column in an image. A larger gradient will result in a bigger difference between the original and resampled image at a given location, since the resampling is essentially an interpolation between the neighboring pixels. Therefore, instead of studying the mean and σ value for the image as a whole, examining the spectral gradient mean and standard deviation as a function of the temperature gradient may prove useful to highlight regions where the impact of the co-registration errors are most significant. The spectral gradient mean function $m(G)$ and the standard deviation function $\sigma(G)$ are defined as

$$m(G) = \frac{1}{N_G}\sum_{i\in G} [T_2(i) - T_4(i)], \tag{18}$$

Table 1 The mean and σ values of the brightness temperature difference between channels 2 and 4 for Geostationary Operational Environmental Satellite images on day 136, 2012 (May 15, 2012). The original and resampled numbers are in K. The co-registration error δ for each image set is also shown.

		M		σ	
Time of the day	δ	Original	Resampled	Original	Resampled
07:15	0.69	5.1420	5.1408	7.9124	7.8337
08:15	0.82	5.6135	5.6117	7.5341	7.4116
09:15	0.99	6.2367	6.2343	7.3505	7.1971
10:15	1.06	6.9814	6.9794	7.4415	7.2777
11:15	1.13	7.5049	7.5029	7.4183	7.2465
12:15	1.17	8.2595	8.2573	7.6698	7.4984
13:15	1.19	9.2032	9.2011	8.1957	8.0367
14:15	1.14	10.2747	10.2728	8.6715	8.5281
15:15	1.05	11.2049	11.2039	8.9768	8.8664
16:15	0.88	12.0516	12.0508	9.4443	9.3547
17:15	0.70	12.2007	12.2001	9.5635	9.4959
18:15	0.51	11.4804	11.4800	9.3268	9.2842

$$\sigma(G) = \sqrt{\frac{1}{N_G}\sum_{i\in G}[T_2(i) - T_4(i) - m(G)]^2}, \tag{19}$$

where the variable G is defined as

$$G = \text{round}[g_2(i)]. \tag{20}$$

The summations in Eqs. (18) and (19) are over those pixels with the same temperature gradient value G, and G is the rounded integer of the temperature gradient for the channel 2 image. The variable N_G in Eqs. (18) and (19) is the number of pixels with the temperature gradient G. The functions $m(G)$ and $\sigma(G)$ are equivalent to the spectral gradient functions in the spatial-spectral gradient representation discussed in Wu et al.[3]

Figure 10 shows the functions $\sigma(G)$ and $m(G)$ for the original and resampled channel 4 images. The function $\sigma(G)$ is essentially the same when the magnitude of temperature gradient G is <2 K, which is due to the fact that changes to the resampled pixels are very small. The changes to both mean and σ functions are more significant as the temperature gradient increases. Since the magnitude of the temperature gradient for the vast majority of the pixels in the images is <2 K, the changes to the overall mean and σ value for the Earth-viewing pixels are small. There are also larger fluctuations as the temperature gradient becomes larger, due to the fact that sample size decreases exponentially as the magnitude of the temperature gradient increases. The number of pixels with a gradient of 0 K is 2.4×10^6 for the channel 2 image, and it decreases exponentially as the magnitude of the gradient increases. The number of pixels with a gradient >16 K is <100, which makes it more dependent on the content of specific images and less meaningful statistically. As the temperature gradient increases, the differences in both the $\sigma(G)$ and $m(G)$ functions between the original and resampled images become much more pronounced.

Figure 10 shows that there are overall reductions in the σ values for the resampled image by as much as 2 K, especially for the positive temperature gradient region, which suggests that the resampled image improves the noise level in the temperature difference significantly. The high

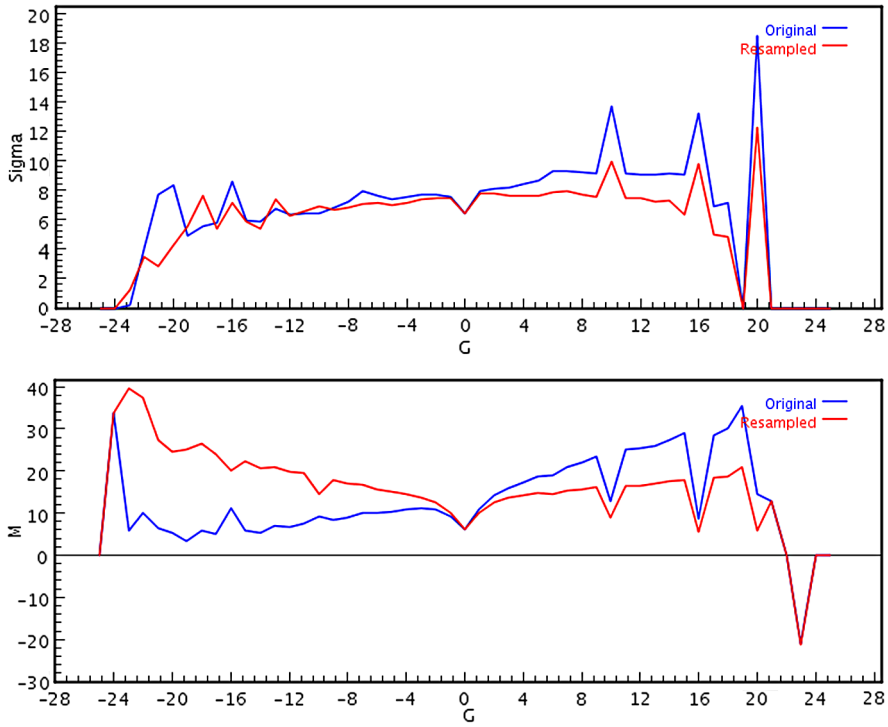

Fig. 10 σ (on the top) and mean (on the bottom) values of the brightness temperature difference between channels 2 and 4 images as a function of the temperature gradient in channel 2. The blue line represents the original channel 4 image shown in Fig. 4, and the red line represents the resampled channel 4 image. The co-registration error is 1.17.

noise level is directly related to the co-registration error between the images in two channels; the larger the misalignment, the bigger the noise level. This shows that using σ as a function of the temperature gradient is an important measure that can be used to verify the output of the channel-to-channel co-registration characterization algorithm.

Although the co-registration error does not change the overall spectral gradient mean values, Fig. 10 shows that the spectral gradient function $m(G)$ for the original imagery is asymmetric between the positive and negative temperature gradients G, in which the mean value for the positive gradient is larger than that for the negative gradient. This is the same asymmetric behavior shown on the spatial-spectral gradient histograms in Refs. 3 and 2, and is caused by the co-registration errors between the channels 2 and 4 images. To show the quantitative relationship between the asymmetry in the spatial-spectral gradient representation and the channel-to-channel co-registration error, one can define a global spatial-spectral gradient asymmetry as

$$\alpha = \sum_{G=1}^{\max|G|} \left[\frac{N_G}{N_P} m(G) - \frac{N_{-G}}{N_N} m(-G) \right], \tag{21}$$

where the $N_p(N_N)$ is the total number of pixels with positive (negative) temperature gradients. Equation (21) is essentially the difference between the mean values of the spectral gradients with positive and negative spatial gradients. The spatial-spectral gradient asymmetry α is a quantitative global measure of the spatial-spectral gradient representation. One can evaluate the asymmetry α for each image data set and compare it with the co-registration error δ from the GII4C algorithm. Figure 11 shows the data points for the asymmetry α (y axis) and the co-registration error δ (x axis) for the image data sets on day 136, 2012 (May 15, 2012), where the co-registration error δ values are obtained from the GII4C algorithm. The results in Fig. 11 show a strong correlation between the co-registration error δ and the asymmetry α for the original imagery. As the co-registration error δ increases, the asymmetry α increases as well. The maximum δ value corresponds to the maximum α value. The asymmetry values for the resampled channel 4 images

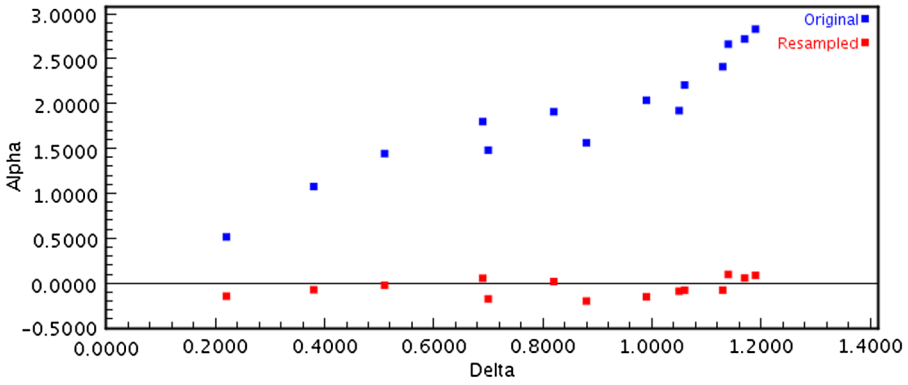

Fig. 11 The asymmetry α versus co-registration error δ. The blue data points represent the spatial-spectral gradient asymmetry between the channel 2 and original channel 4 images, and the red data represent the spatial-spectral gradient asymmetry between the channel 2 and resampled channel 4 images. The asymmetry α has the unit K.

are consistently around 0, which suggests that the co-registration errors between the channels 2 and 4 images are mostly corrected. This shows that the spatial-spectral gradient asymmetry α can be a very effective global metric to evaluate the effectiveness of channel-to-channel co-registration characterization algorithms.

The effects of the spectral gradient functions $m(G)$ and $\sigma(G)$ are also shown in local features. Figure 12 shows the effects of the reduction of the σ value on the temperature difference surface. The image on the top represents the temperature difference between the channel 2 and original channel 4 image, while the image on the bottom shows the temperature difference between the channel 2 and the resampled channel 4 image. The surface of the temperature difference between the channel 2 and resampled channel 4 images is smoother. The maximum value of the temperature difference in like regions is reduced by ~5 K, while the minimum value is increased by ~2.6 K. The variations on the temperature difference surface with the original channel 4 image result from noises caused by the co-registration error.

Figure 13 highlights how the asymmetric behavior shown in Fig. 10 is related to the co-registration error. The figure displays the temperature difference between channels 2 and 4 in the Great Lakes region, which is a subset of the images shown in Figs. 3 and 4. The lake boundaries in Fig. 13 have large temperature gradients, where the changes made by the image resampling are

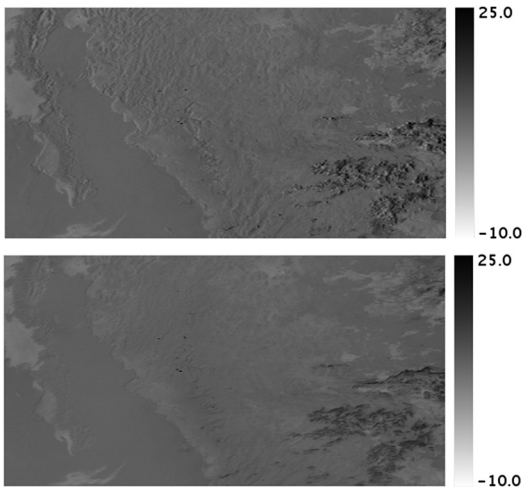

Fig. 12 Temperature difference between the channel 2 and 4 images. The Gulf of California can be seen in the lower left hand corner of each image. The top image is the difference between the channel 2 and original channel 4 images, while the bottom image corresponds to the difference between the channel 2 and resampled channel 4 images.

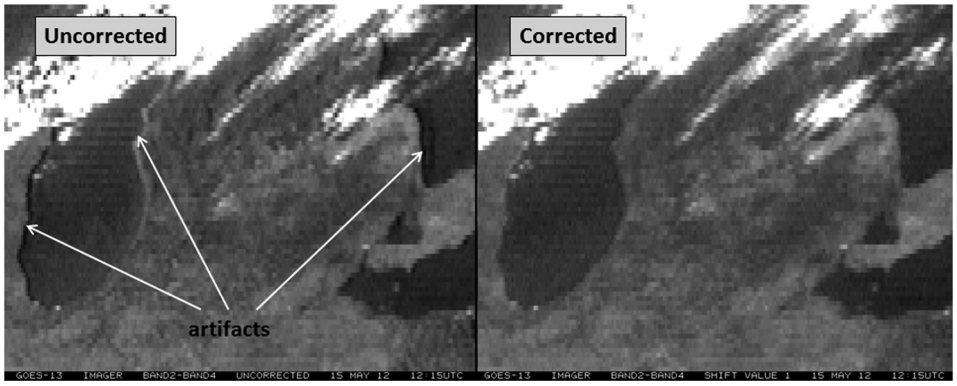

Fig. 13 Temperature difference between channels 2 and 4 in the vicinity of lakes Michigan, Huron, and Erie.

most significant. The temperature gradient on the west side of the lake boundary is negative, so Fig. 13 suggests a lower than normal temperature difference, which is manifested as a darker edge along the lake boundary. On the east side of the lake boundary, the temperature gradient along the west/east direction is positive, and the temperature differences for the misaligned channels 2 and 4 images are higher than the normal value, which is manifested as the whiter edge along the lake boundary on the east side. These are artifacts caused by large co-registration errors and lead to false positives in fog detection, for example. The artifacts along the lake boundary are largely removed after resampling, in which the resampled channel 4 image is shifted west by 1.17 pixels.

Figures 12 and 13 verify the veracity of the GII4C algorithm based on local features, and they also provide important empirical evidence in support of using both the spatial-spectral gradient asymmetry α and spectral gradient function $\sigma(G)$ as global metrics showing image co-registration errors.

6 Implementation of the GII4C Algorithm in the GOES Ground System

There are two components involved in implementing the GII4C algorithm in the GOES ground system. The first is an offline program that implements the GII4C algorithm to determine the (time-dependent) co-registration error; the second is a real-time program to correct the co-registration errors in GOES images based on the output from the offline program.

The offline program of the GII4C algorithm evaluates every image during a five-day period (~400 images). Figure 14 shows the co-registration errors for the IR channel-to-channel co-registration as a function of time for both the east/west and north/south directions for GOES-13. The data have a pattern that repeats every 24 h. The maximum co-registration error is ~1.2 pixels for the co-registration between channels 2 and 4. The results in Fig. 14 show that the co-registration error in the north-south direction is generally small and that the dependence on time is not as strong as that observed in the east-west direction. The magnitude of the co-registration error in the east-west direction between channels 2 and 4 is >0.5 pixels during several periods each day, which requires image resampling in either channel 2 or channel 4 for corrective purposes. This is in good agreement with the results from the approach presented in Ref. 2.

There are still fluctuations in co-registration errors from one image to another, due to the fact that the brightness temperature correlation is essentially a statistical approach. The final co-registration error values are obtained through a least squares fit to the time-dependent function.

$$P(t) = P_0 + \sum_{k=1}^{N} \left[P_k^s \sin\left(\frac{2\pi kt}{24}\right) + P_k^c \cos\left(\frac{2\pi kt}{24}\right) \right], \tag{21}$$

where P_0, P_k^s, and P_k^c are the parameters used in the least squares fit. $N = 5$ is used in the least squares fit in Fig. 14, which corresponds to 11 parameters. In practice, the time-dependent function, $P(t)$, in Eq. (21) is used to generate a co-registration table (CORT). The CORT in the east/west direction, generated from the co-registration error results in Fig. 14, is shown in Fig. 15.

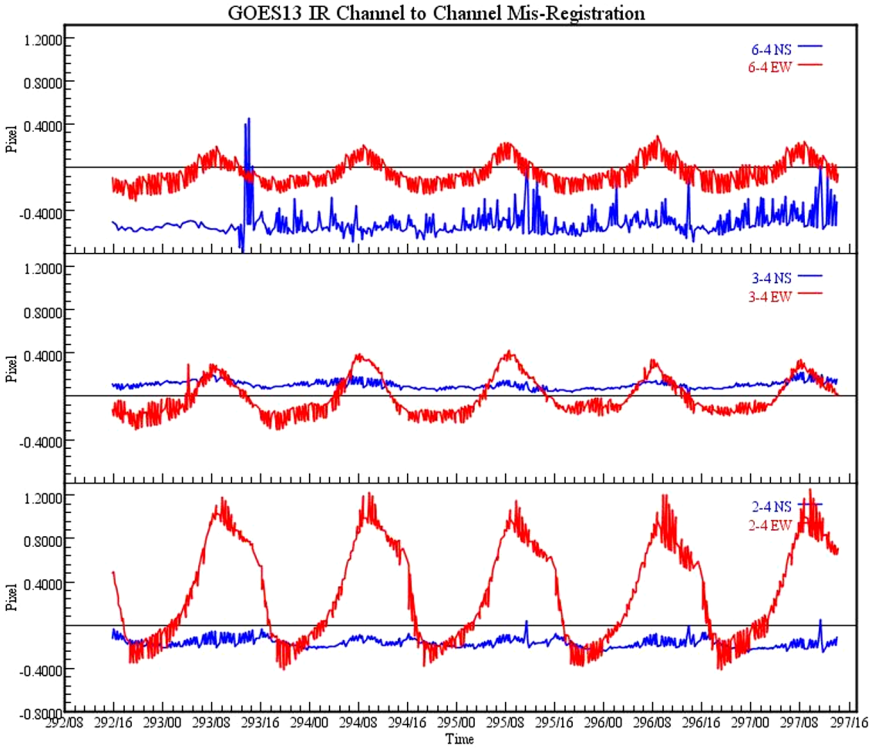

Fig. 14 The east-west (in red) and north-south (in blue) channel-to-channel co-registration error for GOES-13 as a function of time.

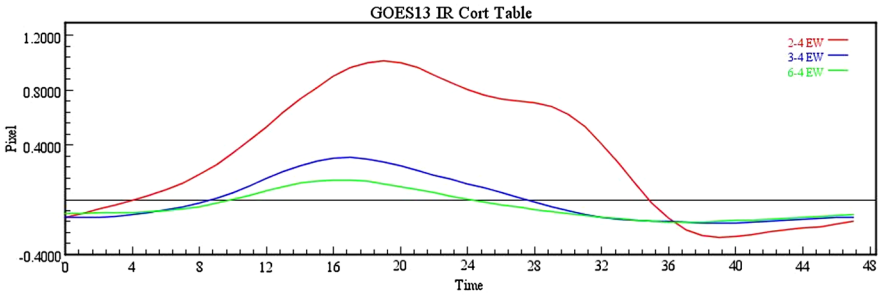

Fig. 15 GOES-13 IR co-registration table for east/west co-registration error values after the least squares fitting. The time axis is half-hourly through the day.

The CORT is an array with 48 elements, in which each element represents the co-registration error during a half-hourly period. The GOES ground system corrects co-registration errors for GOES imagery based on the CORT. There are seasonal changes for the CORT; therefore, it is updated on a monthly basis.

7 Summary

The GII4C algorithm presented in this paper provides a systematic approach to characterize the co-registration errors for the GOES Imager IR channels. The algorithm is an area-based approach, and it evaluates the correlation of the brightness temperatures between different IR channels. The algorithm does not depend on a few CP, so it is not impacted by the presence of clouds. In fact, clouds are one of the features in IR channel imagery that enhance the correlation. An FFTR algorithm is used for the image resampling in order to obtain the co-registration errors at a subpixel level. The results presented have shown very high correlation values, a

continuous correlation as a function of the imagery shifts, and a stable co-registration error output, which ensures the stability and reliability of the algorithms.

Because the images in different IR channels are not related by an affine transformation, there is no controlled experiment to determine the accuracy of the algorithm. Validation of the algorithms is a combination of global measures and their related local features. Since changes by the image resampling are most significant in regions where the temperature gradients are large, we show that the spectral gradient mean and σ function between the IR channels can be used to highlight the effects of the co-registration errors. Larger co-registration errors lead to larger σ values, especially in those areas where temperature gradients are large. The co-registration error does not change the overall spectral gradient mean value; however, it causes an asymmetric behavior in the function $m(G)$ [Eq. (18)], which is the same as the asymmetry in the spatial-spectral histogram(s) shown in Ref. 3. We propose that the spatial-spectral gradient asymmetry α and the spectral gradient function $\sigma(G)$ are quantitative global measures to verify the channel-to-channel co-registration errors, which can be useful metrics to evaluate channel-to-channel co-registration characterization algorithms. We showed that the spatial-spectral gradient asymmetry α and the co-registration error δ are strongly correlated. Further investigation is needed to determine the quantitative relationship between α and δ.

Both global measures and local features have shown that the co-registration errors between GOES-13 Imager 3.9 and 10.7 μm data are largely removed by the image resampling based on the output of the GII4C algorithm. The quality of the associated weather products should be improved significantly.

The GII4C algorithm has been implemented in the operational GOES ground system. The same approach could also be applicable to the next generation of GOES.

Acknowledgments

The contents of this document are solely the opinions of the authors and do not constitute a statement of policy, decision, or position on behalf of NOAA or the U.S. Government.

References

1. G. P. Ellrod, "Advances in the detection and analysis of fog at night using GOES multispectral infrared imagery," *Weather Forecast.* **10**, 606–619 (1995).
2. M. G. Grotenhuis et al., "On orbit characterization of the GOES Imager channel to channel co-registration," *Proc. SPIE* **8510**, 85101T (2012).
3. X. Wu, W. P. Menzel, and W. L. Smith, "Impact of the new generation GOES on the determination of sea surface temperature," *Proc. SPIE* **2812**, 84–94 (1996).
4. J. Le Moigne, N. El-Saleous, and E. Vermote, "Iterative edge- and wavelet-based image registration of AVHRR and GOES satellite imagery," in *Image Registration Workshop Proc.*, pp. 137–146, NASA, GSFC, Greenbelt, Maryland (1997).
5. Z. Li, "The fast Fourier transformation resampling algorithm and its application in satellite image processing," *J. Appl. Remote Sens.* **8**(1), 083683 (2014).
6. H. Stone et al., "A fast direct Fourier-based algorithm for subpixel registration of images," *IEEE Trans. Geosci. Remote Sens.* **39**(10), 2235 (2001).
7. W. H. Press et al., *Numerical Recipes in C*, Cambridge Press, Cambridge, UK (1992).
8. M. Grotenhuis et al., "On-orbit characterization of the GOES Imager channel-to-channel co-registration and correction algorithm evaluation," April 2013, http://satelliteconferences.noaa.gov/2013/docs/Tuesday%20Poster%20Session%20Final%20Posters/T26_Grotenhuis_NOAA_Sat_Conf_2013_GOES_coreg_poster_final_ver3.pdf (9 April 2013).
9. Boeing Technical Report, "GOES N data book," http://rsd.gsfc.nasa.gov/goes/text/goes.databookn.html (2005).
10. W. K. Pratt, "Correlation technique of image registrations," *IEEE Trans. Aerosp. Electron. Syst.* **AES-10**(3), 353–358 (1974).
11. M. P. Weinreb, J. X. Johnson, and D. Han, "Conversion of GVAR Infrared Data to Scene Radiance or Temperature," NOAA Technical Memorandum, NOAA NESDIS Office of Satellite Operations (2006).

12. NOAA Technical Report, "Earth location user's guide," http://goes.gsfc.nasa.gov/text/ELUG0398.pdf (1998).

Zhenping Li received a PhD degree in physics at the University of Tennessee, and a master's degree in computer science at Johns Hopkins University. Currently he is working at ASRC Federal as the systems engineer. His research area is satellite image processing and its implementation in the satellite ground system.

Michael Grotenhuis is a physical scientist and an ERT, Inc. contractor at the NOAA/NESDIS Center for Satellite Applications and Research (STAR). Currently, he supports calibration/validation efforts to monitor the instrument performance of the Ozone Mapping Profiler Suite using the Satellite Integrated Calibration/Validation System (ICVS). He received a BA in physics from Cornell University in 2003 and an MS in physics from the University of Minnesota—Twin Cities in 2010.

Xiangqian Wu has been a physical scientist with the National Oceanic and Atmospheric Administration (NOAA) in Maryland, USA, since 2002, where he leads a team to provide calibration support for NOAA's operations of Imager and Sounder on GOES and AVHRR on POES. From 2010 to 2014, he led a team for the instrument calibration and validation of OMPS on Suomi-NPP. Currently, he leads a team for the instrument calibration and validation of ABI on GOES-R.

Timothy J. Schmit works at the Advanced Satellite Products Branch within NOAA's NESDIS Center for Satellite Applications and Research located in Madison, Wisconsin. His experience with satellite processing includes calibration, simulations and algorithms for converting satellite data into meteorological/environmental information. He has extensive experience with deriving products from the GOES imager and sounder data. He was involved in the on-orbit science check-out of GOES-8 through 15. He received his master's degree from the University of Wisconsin—Madison.

Chris Schmidt: Biography is not available.

Anthony J. Schreiner works at the University of Wisconsin Cooperative Institute for Meteorological Satellite Studies at Madison, Wisconsin. His experience with satellite information includes developing algorithms for converting satellite data into meteorological/environmental information and product assurance for both the GOES imager and sounder. He was involved in the development and implementation of the algorithm for generating cloud information from both the GOES sounder and imager in order to enhance the National Weather Service Automated Surface Observing System. Anthony received his bachelor's and master's degree in meteorology from the University of Wisconsin—Madison.

James P. Nelson III works at the Cooperative Institute for Meteorological Satellite Studies, located in Madison, Wisconsin. He has extensive experience working with geostationary satellite data and other types of surface and upper air-based meteorological data, mainly in the realm of diagnostic and value-added software development. He has contributed to the on-orbit science check-out of numerous GOES satellites, and focuses on data quality-control. He received his master's degree from the University of Wisconsin—Madison.

Fangfang Yu received a BS degree and MS degree from Peking University, Beijing, China, in 1991 and 1994, respectively, and a PhD degree in geography from the University of Kansas, Lawrence, in 2002. She has been supporting the GOES weather instrument calibration and validation at NOAA/NESDIS since 2007.

Hyre Bysal is Geostationary Environmental Satellite (GOES) payload operations lead engineer at NOAA/NESDIS/OSPO in Suitland, Maryland, since 2002. After four years in nuclear industry, Hyre worked at Honeywell, and Motorola as Six-Sigma process specialist. He then moved to Motorola-Iridium project for satellite manufacturing, integration and launch optimization, which led him to NOAA GOES satellites. He received his bachelor's degree from Bosphorus University in Istanbul, Turkey, and his master's degree from the University of Kentucky.